Direct laser writing of three-dimensional photonic-crystal templates for telecommunications

MARKUS DEUBEL[1], GEORG VON FREYMANN[1], MARTIN WEGENER[2], SURESH PEREIRA[3], KURT BUSCH[3,4] AND COSTAS M. SOUKOULIS[5]

[1]Institut für Nanotechnologie, Forschungszentrum Karlsruhe in der Helmholtz-Gemeinschaft, D-76021 Karlsruhe, Germany
[2]Institut für Angewandte Physik, Universität Karlsruhe (TH), Wolfgang-Gaede-Straße 1, D-76131 Karlsruhe, Germany
[3]Institut für Theorie der Kondensierten Materie, Universität Karlsruhe (TH), Wolfgang-Gaede-Strasse, D-76128 Karlsruhe, Germany
[4]Department of Physics and School of Optics: CREOL & FPCE, University of Central Florida, Orlando, Florida 32816, USA
[5]Ames Laboratory and Department of Physics and Astronomy, Iowa State University, Ames, Iowa 50011, USA
*e-mail: soukoulis@ameslab.gov

Published online: 13 June 2004; doi:10.1038/nmat1155

The past decade has witnessed intensive research efforts related to the design and fabrication of photonic crystals[1,2]. These periodically structured dielectric materials can represent the optical analogue of semiconductor crystals, and provide a novel platform for the realization of integrated photonics. Despite intensive efforts, inexpensive fabrication techniques for large-scale three-dimensional photonic crystals of high enough quality, with photonic bandgaps at near-infrared frequencies, and built-in functional elements for telecommunication applications, have been elusive. Direct laser writing by multiphoton polymerization[3] of a photoresist has emerged as a technique for the rapid, cheap and flexible fabrication of nanostructures for photonics. In 1999, so-called layer-by-layer[4] or woodpile photonic crystals were fabricated with a fundamental stop band at 3.9 μm wavelength[5]. In 2002, a corresponding 1.9 μm was achieved[6], but the important face-centred-cubic (f.c.c.) symmetry was abandoned. Importantly, fundamental stop bands or photonic bandgaps at telecommunication wavelengths have not been demonstrated. In this letter, we report the fabrication—through direct laser writing—and detailed characterization of high-quality large-scale f.c.c. layer-by-layer structures, with fundamental stop bands ranging from 1.3 to 1.7 μm.

Since the introduction of the concept of three-dimensional (3D) photonic crystals (PCs) and photonic bandgap (PBG) materials, scientists have dreamed of realizing photonic circuits in analogy to semiconductor electronics. This poses a major technological challenge for nanofabrication. On the one hand, for telecommunication applications, PCs with lattice constants of the order of several hundreds of nanometres have to be realized with sub-10-nm precision. On the other hand, the complete structures have to cover substantial fractions of a square millimetre or more to accommodate a photonic circuit. Moreover, the dielectric used has to have a large refractive index to open a PBG. Different approaches have been used to tackle this challenge.

Large PBGs (theoretically up to 25% of the centre frequency for silicon[7]) can be realized with PCs exhibiting diamond symmetry.

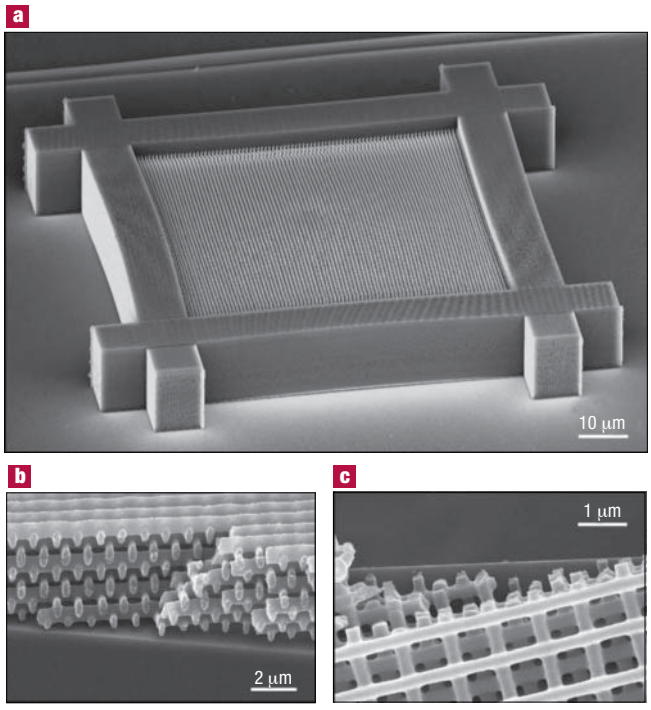

Figure 1 Three-dimensional photonic crystals fabricated by DLW. a, Layer-by-layer structure with 40 layers and a massive wall that prevents bending and reduces distortions due to polymer shrinkage during polymerization, completely fabricated by DLW. **b**, Side and **c**, top view of a different broken sample with 12 layers, illustrating the sample quality obtained with the DLW process.

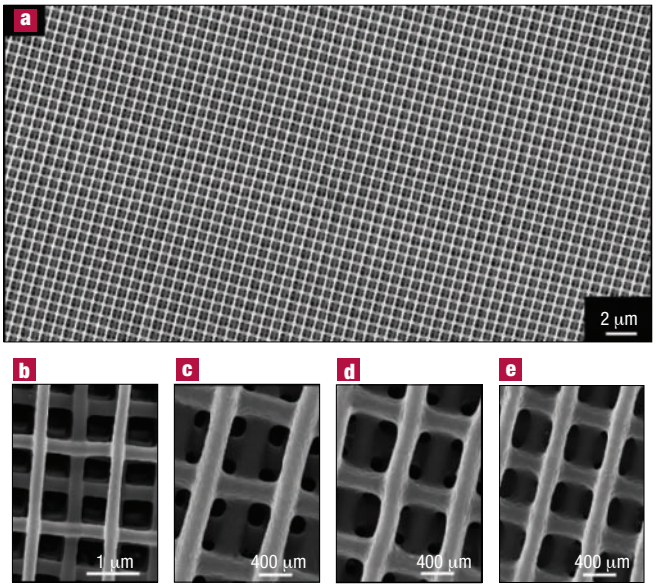

Figure 2 Examples of different lattice constants. a, The panorama view of a sample with rod spacing $a = 0.65$ μm reveals the large-scale periodicity of our samples, whereas close-ups for samples with different rod spacings exhibit the small-scale fabrication accuracy: **b**, $a = 1.5$ μm, **c**, $a = 1.0$ μm, **d**, $a = 0.8$ μm, and **e**, $a = 0.65$ μm. For all samples $(c/a)^2 = 2$.

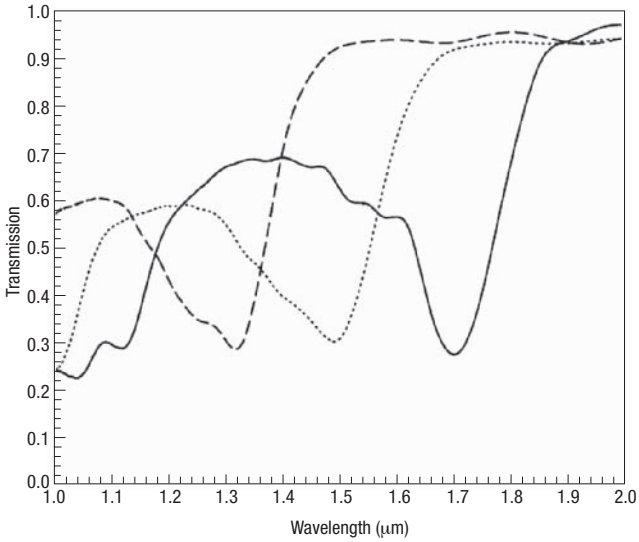

Figure 3 Optical transmission spectra of samples with different in-plane rod spacings. Transmission spectra of three different layer-by-layer samples with in-plane rod spacings of $a = 1.0$ μm (solid line), $a = 0.9$ μm (dotted line), and $a = 0.8$ μm (dashed line).

In particular, the layer-by-layer structure is amenable to microfabrication techniques, and PBGs at infrared frequencies have been realized through combinations of advanced planar semiconductor microstructuring techniques for individual layers with sophisticated alignment and stacking procedures to combine different layers into 3D PCs[8–10]. These technologically very demanding approaches offer the incorporation of functional elements through controlled modifications in individual layers. However, to date, successful stacking has been reported for a few layers only. This rather limited size leads to a strong coupling between the guiding modes required for the operation of functional elements embedded in these PCs to the leaky modes of the material surrounding the PC structure. As a result, the performance of these functional elements is compromised. Therefore, researchers have recently pursued the infilling of high-index materials into template structures. Two possibilities to fabricate such templates have been discussed. (1) Self-assembly of colloidal particles: The fabrication and infiltration of opal-type templates by self-assembly has successfully been demonstrated[11,12]. However, the self-organising nature of this assembly process almost inevitably leads to the formation of unwanted defects, such as missing particles (cavities), dislocations (grain boundaries) and so on. The resulting PCs exhibit f.c.c. symmetry and possess relatively small PBGs (theoretically up to 9% of the centre frequency for silicon inverse opals[13]), which are rather susceptible to surface roughness and other fabrication tolerances. (2) Nanolithography of photoresists: Two complementary and compatible techniques, namely holographic lithography and direct laser writing (DLW), can deliver photoresist templates. Holographic lithography is capable of providing defect-free films with thicknesses of several tens of unit cells and lateral extents of several square millimetres, and offers a tremendous flexibility in tailoring the interior of the unit cell[14,15]. Provided that the same photoresist is used, functional elements such as waveguides and micro-cavities can be inscribed in a second exposure step by DLW. Alternatively, also complete PCs can be written by DLW.

In DLW by multiphoton polymerization, a photoresist is illuminated by laser light at a frequency below the single-photon polymerization threshold of the resist. When this laser light is tightly focused inside the photoresist, the light intensity inside a small volume (the focus) may exceed the threshold for initiating multiphoton polymerization. The size and shape of these so-called voxels depend on the iso-intensity surfaces of the microscope objective, and the exposure threshold for multiphoton processes of the photosensitive medium. To date, lateral voxel sizes down to 120 nm for illumination at a wavelength of 780 nm have been reported[3].

A key part of our work is that we use the commercially available thick-film negative photoresist SU-8 in the DLW process (see Methods). This allows SU-8-based holographic lithography techniques to be combined with the DLW approach. This compatibility of holographic lithography and DLW is crucial when realizing large-scale PC circuits, and is facilitated by the cationic polymerization mechanism of SU-8, in which monomers do not directly polymerize after exposure. Therefore, the difference in refractive indices of exposed and unexposed regions of the resist are negligible, and structures that have already been exposed do not affect further exposure steps. In addition, SU-8 remains solid during the writing process. This eases the sample handling and provides the flexibility needed for realizing complex, physically disconnected functional elements such as coupled cavity/waveguide systems. As a result, when working with SU-8, DLW may be added as a second exposure step to the holographic lithography process, and may be studied and optimized independently.

Owing to its geometrical simplicity, the layer-by-layer PCs we fabricate represent ideal test structures for DLW. They consist of stacks of parallel rods with period a. These rods are built up from joining individual voxels that are each exposed by a single laser pulse, such that the rod cross-section is determined by the shape of these voxels. For laser light of 800 nm wavelength and a microscope objective with a numerical aperture of 1.4, we expect a near-elliptical cross-section with an aspect ratio (axial diameter/lateral diameter) of about 2.7. The absolute dimension of the voxels can be adjusted through the single pulse energy of the laser light, with higher energy leading to larger voxels. Rods in successive layers are rotated by an angle θ relative to each other. In our

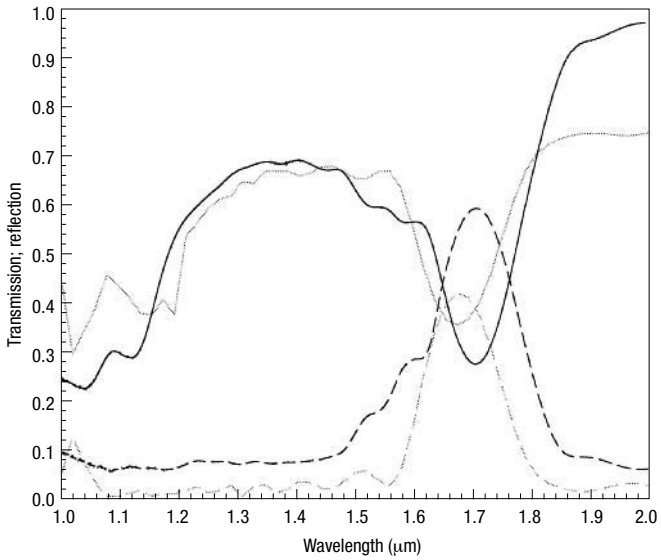

Figure 4 Comparison of experiment and simulation. Transmission (solid curves) and reflection (dashed curves) spectra from experiment (black) and theory (grey). The rod spacing is $a = 1.0$ μm (solid line in Fig. 3) and $(c/a)^2 = 2$. Note the good overall agreement.

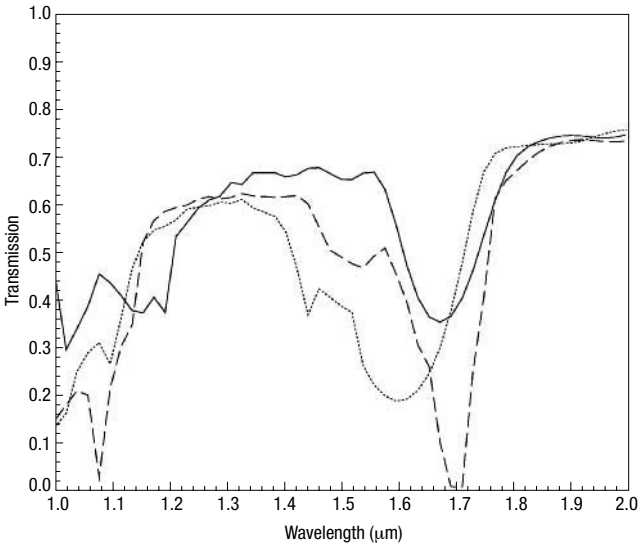

Figure 5 Angular dependence of photonic-crystal transmission. Simulated transmission spectra for three different angles of incidence. Normal incidence (solid curve), 20° (dotted curve) and 30° (dashed curve). The other parameters correspond to Fig. 4.

experiment, $\theta = 90°$ but, in general, could vary between 60–90° and still produce a PBG after infiltration[16]. Second nearest-neighbour layers are displaced by $a/2$ relative to each other. Four layers form a lattice constant c. For $(c/a)^2 = 2$, this 3D lattice exhibits an f.c.c. unit cell with a two-rod basis and can be derived from a diamond lattice by replacing the (110) chains of lattice points with rods[4]. For our parameters, the lateral rod diameters are typically in the range of 180 nm to 250 nm. Figure 1a shows a scanning electron microscope (SEM) image of a typical sample consisting of 40 layers with an in-plane rod distance of $a = 0.8$ μm and $(c/a)^2 = 2$. The fabrication time for this lattice was approximately 25 minutes. A massive wall has been written around the PC by the same technique to avoid sample bending due to polymer shrinkage during the development process. Furthermore, lattice distortions, which would otherwise strongly influence the entire sample, are limited to the very border zones. One gets a feeling for the enormous strain by looking at the bowing of the wall, for example, visible on the left side. Without such walls, this stress would largely deteriorate the quality of the PC template. Figure 1b and c are SEM images of the edge and top of a different broken sample that show the elliptical rod cross-section and the layer-by-layer stacking sequence, revealing the quality of our samples.

With the flexibility of the DLW approach, we can fabricate a wide variety of lattice parameters and filling fractions. Figure 2 gives an overview over several samples that we have fabricated. The in-plane rod distances here range from 1.5 μm to 0.65 μm. In the close-ups at the bottom, a remaining roughness of the order of 10 nm is visible. The same roughness is also apparent from our SU-8 templates fabricated by holographic lithography[15]. This clearly indicates that this roughness is not due to the fabrication process but rather stems from the finite resolution of the photoresist.

To move the fundamental PBGs to wavelengths in the telecommunication regime of 1.5 μm and 1.3 μm, it is necessary to have an in-plane rod spacing of the order of 1 μm and smaller. Therefore, we prepared samples with rod spacing of 1.0 μm, 0.9 μm and 0.8 μm, all samples with 24 layers and $(c/a)^2 = 2$. The sample area of 100 μm × 100 μm is sufficiently large for optical spectroscopy as well as for potential devices. It is clear that the midgap wavelength will move towards longer wavelengths after infiltration of the template by a high-index material (for example, silicon). More precisely, band-structure calculations[16] show that the maximum gap-to-midgap ratio at 1.5-μm midgap wavelength is achieved for a rod width of 200 nm and a silicon rod spacing of $a = 0.72$ μm, corresponding to a silicon filling ratio of 28%. We have also successfully fabricated samples with $a = 0.5$ μm and $(c/a)^2 = 2$. However, at this point, the rods start to touch each other, leading to an undesirably large filling fraction. This could, in principle, be compensated for by reducing the laser pulse energy during exposure, but this makes the process more susceptible with respect to fluctuations of the laser. Also, the resolution of SU-8 plays an important role, as rod diameters of the order of 100 nm are produced—a size that starts to become comparable with the roughness already mentioned above. This problem could be overcome by reducing the rod diameter, hence the filling fraction, after the development process by etching in an oxygen plasma (G. von Freymann, *et al.* unpublished work).

Figure 3 shows the measured transmission spectra for three different samples with $a = 1.0$, 0.9 and 0.8 μm and an estimated SU-8 filling fraction of about 35% in each case. The corresponding fundamental stop bands are clearly visible as pronounced dips in transmission and shift from 1.7 μm, to 1.5 μm, and then to 1.3 μm. Higher-order stop bands are also observed (not shown). In independent experiments on polymerized bulk SU-8 films of comparable thickness, we observe a transmission close to 100% throughout the entire wavelength range shown in Fig. 3. This indicates that none of the spectral features shown can be attributed to absorption effects in the polymer.

Figure 4 shows both transmission and reflection spectra (black curves) for the sample with a rod spacing $a = 1.0$ μm (corresponding to the solid curve in Fig. 3). We now compare these measurements with theory (grey curves). The agreement between the two can be regarded as a measure of the quality of our structures. To make this comparison as direct as possible, we actually account for the elliptical shape of the rods, for example, visible in Fig. 1, through an appropriate discretization. The surface roughness of the rods leads to scattering. This is accounted for by phenomenologically introducing a complex index of refraction (see Methods). The overall agreement between simulations and

measurements is very good and almost quantitative. This, together with a sufficiently low value of the imaginary part of the index of refraction underlines the very high optical quality of our samples. To further appreciate the level of agreement, and to investigate the remaining minor deviations in detail, we consider in Fig. 5 the influence of different angles of incidence in the simulations (unpolarized light). A superposition of different angles would mimic the peculiarities of the actual measurement (see Methods), which does not use incident plane waves but rather uses a Cassegrain objective with numerical aperture of 0.5, corresponding to 30° opening angle. An angle of 30° in the transmission data of Fig. 5 even reproduces the small features on the short-wavelength side of the fundamental stop band. A yet more detailed comparison of experiment and simulation in Fig. 4 shows that the experimental transmission is larger than the theoretical one on the long-wavelength side of the fundamental stop band. This indicates that the description of scattering losses in terms of a frequency-independent imaginary part of the refractive index has its limitations. Actually, one would have to account for the nano-roughness on a 10-nm scale.

We currently envision inverting these 3D PC templates by a two-step process: In a first step, the templates would be infiltrated with SiO_2, followed by subsequent removal of the SU-8. In a second inversion step, silicon would be infiltrated and the SiO_2 etched away. This would result in a positive replica of the polymer template. Under these conditions, the lattice constants achieved allow for complete PBGs near telecommunication wavelengths. The combination with holographic lithography facilitates the rapid, flexible and cheap fabrication of 3D PCs, as well as the controlled incorporation of defects and waveguides.

METHODS

The commercially available photoresist SU-8 (MicroChem) consists of an octafunctional epoxy resin (EPON SU-8), a photoinitiator (mixed triarylsulphonium/hexafluoroantimonate salt in propylene carbonate solvent), both dissolved in gamma-butyrolactone (GBL). On irradiation by near-ultraviolet light (350–400 nm), the photoinitiator generates an acid with a spatial concentration that is an image of the irradiation dose. In a post-exposure bake, the latent image is converted into a crosslinking density by a chain reaction. The crosslinking degree determines the solubility in the 'developing' solvent. GBL or another appropriate solvent is used in this step. Thus, sufficiently illuminated resin remains ('negative' photoresist) whereas the underexposed resin is washed out. For our experiments, photoresist samples are prepared by spin-coating SU-8 films on microscope cover slides. After evaporation of the solvent in a soft-bake step at 65 °C, a 20-μm-thick film results. To write PC structures into these films, we use a regeneratively amplified Ti:sapphire laser system (Spectra Physics Hurricane) with a pulse duration of 120 fs. The repetition rate can be computer controlled from 1 kHz to single shot mode. The wavelength is tuned to 800 nm, where the one-photon absorption of the photoresist is negligible. The output beam is attenuated by a half-wave plate/polarizer combination, and after beam expansion, typically a few tens of nanojoules of single pulse energy are coupled into an inverted microscope (Leica). There, the femtosecond pulses are focused into the photoresist sample by a ×100 oil immersion objective (Leica, numerical aperture of 1.4). The sample is placed on a three-axis piezoelectric scanning stage (Physik Instrumente), which is operated in closed loop and provides a resolution of better than 5 nm at a full scanning range of 200 μm × 200 μm × 20 μm. A personal computer controls the scanning operation of the piezo and synchronizes its movement with the output of the laser system. After DLW of the preprogrammed pattern, the exposed sample is post-baked with a temperature ramp from 65 to 95 °C for six minutes, and developed for one hour in the SU-8 developer, resulting in a positive image of the scanned pattern.

Transmission and reflection spectra are measured with a Fourier-transform infrared spectrometer (Bruker Equinox 55, NIR halogen source) combined with an infrared microscope (Bruker Hyperion 2000, ×36 Cassegrain objectives, numerical aperture of 0.5, liquid-N_2-cooled InSb detector). The samples are aligned with their surfaces perpendicular to the optical axis, which corresponds to the Γ-X direction for f.c.c. symmetry. A circular area with 50 μm diameter is defined by an aperture in the light path of the microscope. The transmission and reflection spectra are normalized to the bare cover slide and a silver mirror, respectively.

We calculate the transmission and reflection spectra from the finite structure using a scattering-matrix technique developed by Whittaker and Culshaw[17], but modified using the suggestions of Li[18] to account more effectively for the complex index of refraction (n). In these scattering-matrix calculations, we account for the light scattering originating from surface roughness by a phenomenological imaginary part of the index of refraction. On this level of description, the imaginary part can be added either to the refractive index of SU-8 or to that of air. We have performed calculations for both choices leading to closely similar results. We obtain the best match to the experiment for $n_{SU\text{-}8} = 1.56$ and $n_{air} = 1.0 + i0.006$ (see Figs 4 and 5) or, alternatively, for $n_{SU\text{-}8} = 1.56 + i0.009$, where i is the imaginary unit, and $n_{air} = 1.0$ (not shown). The lack of a significant difference between the two choices results from the fact that the modes are not well localized either in the dielectric material or in air.

Received 17 December 2004; accepted 21 April 2004; published 13 June 2004.

References

1. Yablonovitch, E. Inhibited spontaneous emission in solid state-physics and electronics. *Phys. Rev. Lett.* **58,** 2059–2062 (1987).
2. John, S. Strong localization of photons in certain disordered dielectric superlattices. *Phys. Rev. Lett.* **58,** 2486–2489 (1987).
3. Kawata, S., Sun, H.-B., Tanaka, T. & Takada, K. Finer features for functional microdevices. *Nature* **412,** 697–698 (2001).
4. Ho, K.-M., Chan, C. T., Soukoulis, C. M., Biswas, R. & Sigalas, M. Photonic band gaps in three dimensions: New layer-by-layer periodic structures. *Solid State Comm.* **89,** 413–416 (1994).
5. Sun, H.-B., Matsuo, S. & Misawa, H. Three-dimensional photonic crystal structures achieved with two-photon-absorption photopolymerization of resin. *Appl. Phys. Lett.* **74,** 786–788 (1999).
6. Straub, M. & Gu, M. Near-infrared photonic crystals with higher-order bandgaps generated by two-photon photopolymerization. *Opt. Lett.* **27,** 1824–1826 (2002).
7. Ho, K.-M., Chan, C. T. & Soukoulis, C. M. Existence of a photonic gap in periodic dielectric structures. *Phys. Rev. Lett.* **65,** 3152–3155 (1990).
8. Lin, S. Y. *et al.* A three-dimensional photonic crystal operating at infrared wavelengths. *Nature* **394,** 251–253 (1998).
9. Noda, S., Tomoda, K., Yamamoto, N. & Chutinan, A. Full three-dimensional photonic bandgap crystals at near-infrared wavelengths. *Science* **289,** 604–606 (2000).
10. Aoki K. *et al.* Microassembly of semiconductor three-dimensional.photonic crystals. *Nature Mater.* **2,** 117–121 (2003).
11. Blanco, A. *et al.* Large-scale synthesis of a silicon photonic crystal with a complete three-dimensional bandgap near 1.5 micrometres. *Nature* **405,** 437–440 (2000).
12. Vlasov, Y. A., Bo, X.-Z., Sturm, J. C. & Norris, D. J. On-chip natural assembly of silicon photonic bandgap crystals. *Nature* **414,** 289–293 (2001).
13. Busch, K. & John, S. Photonic band gap formation in certain self-organizing systems. *Phys. Rev. E* **58,** 3896–3908 (1998).
14. Campbell, M. *et al.* Fabrication of photonic crystals for the visible spectrum by holographic lithography. *Nature* **404,** 53–56 (2000).
15. Miklyaev, Yu. V. *et al.* Three-dimensional face-centered-cubic photonic crystal templates by laser holography: fabrication, optical characterization, and band-structure calculations. *Appl. Phys. Lett.* **82,** 1284–1286 (2003).
16. Biswas, R., Chan, C. T., Sigalas, M., Soukoulis, C. M. & Ho, K.-M. in *Photonic Band Gap Materials* (ed. Soukoulis, C. M.) 23–40 (NATO Science Series E, Vol. 315, Kluwer Academic, Dordrecht, 1996).
17. Whittaker, D. M. & Culshaw, I. S. Scattering-matrix treatment of patterned multilayer photonic structures. *Phys. Rev. B* **60,** 2610–2618 (1999).
18. Li, L. Use of Fourier series in the analysis of discontinuous periodic structures. *J. Opt. Soc. Am. A* **13,** 1870–1876 (1996).

Acknowledgements

We acknowledge the support by the Center for Functional Nanostructures (CFN) of the Deutsche Forschungsgemeinschaft (DFG) within project A.1.2 and A.1.4. The research of K.B. is further supported by DFG-project Bu 1107/2-3 (Emmy-Noether program), that of M.W. by the DFG-Leibniz award 2000 and that of C.M.S. by the Alexander von Humboldt senior-scientist award 2002, and by the US Department of Energy.
Correspondence and requests for materials should be addressed to C.M.S.

Competing financial interests

The authors declare that they have no competing financial interests.